GMFβ controls branched actin content and lamellipodial retraction in fibroblasts

Elizabeth M. Haynes,[1,2] Sreeja B. Asokan,[1,2] Samantha J. King,[1,2] Heath E. Johnson,[4] Jason M. Haugh,[4] and James E. Bear[1,2,3]

[1]UNC Lineberger Comprehensive Cancer Center, The University of North Carolina at Chapel Hill, Chapel Hill, NC 27514
[2]Department of Cell Biology and Physiology and [3]Howard Hughes Medical Institute, The University of North Carolina at Chapel Hill, Chapel Hill, NC 27599
[4]Department of Chemical & Biomolecular Engineering, North Carolina State University, Raleigh, NC 27695

The lamellipodium is an important structure for cell migration containing branched actin nucleated via the Arp2/3 complex. The formation of branched actin is relatively well studied, but less is known about its disassembly and how this influences migration. GMF is implicated in both Arp2/3 debranching and inhibition of Arp2/3 activation. Modulation of GMFβ, a ubiquitous GMF isoform, by depletion or overexpression resulted in changes in lamellipodial dynamics, branched actin content, and migration. Acute pharmacological inhibition of Arp2/3 by CK-666, coupled to quantitative live-cell imaging of the complex, showed that depletion of GMFβ decreased the rate of branched actin disassembly. These data, along with mutagenesis studies, suggest that debranching (not inhibition of Arp2/3 activation) is a primary activity of GMFβ in vivo. Furthermore, depletion or overexpression of GMFβ disrupted the ability of cells to directionally migrate to a gradient of fibronectin (haptotaxis). These data suggest that debranching by GMFβ plays an important role in branched actin regulation, lamellipodial dynamics, and directional migration.

Introduction

Cell migration is fundamental to organismal development and survival, playing a critical role in processes ranging from neuronal development to wound healing. When cell migration goes awry, developmental defects and disease can occur. Problems in cell migration occur not only through failures in motility, but also through failure to recognize and respond to directional cues such as growth factors or ECM. Effective cell migration relies on proper regulation and coordination of actin networks. One such actin population is the branched actin network generated by the Arp2/3 complex (Pollard, 2007). Branched actin is found in the lamellipodium and is generated by activation of Arp2/3 by nucleation-promoting factors (NPFs) like SCAR/WAVE and WASP (Rotty et al., 2013). Once active, Arp2/3 can nucleate a "daughter" filament at a characteristic angle of ∼78° from the original "mother filament" (Rouiller et al., 2008).

The process of branched actin generation has been well studied, but less is known about how branched actin is disassembled. Coronin 1B was identified as having debranching activity through antagonizing the branch-stabilizing protein cortactin, as well as destabilizing the branch itself (Cai et al., 2007, 2008). Coronin 1B has also been found to regulate ADF/cofilin activity at the leading edge via the slingshot phosphatase (Cai et al., 2007). Cofilin binds to actin filaments and severs them at low filament occupancy, but in vitro work shows that high occupancy of a filament by cofilin causes Arp2/3 debranch-ing (Chan et al., 2009). Recently, the cofilin-related protein glia maturation factor (GMF) has been implicated in Arp2/3 regulation (Lim et al., 1989; Gandhi et al., 2010; Ydenberg et al., 2013; Luan and Nolen, 2013).

Unlike cofilin, GMF has no actin binding or severing activity in in vitro assays (Gandhi et al., 2010; Nakano et al., 2010). However, addition of yeast GMF1 to prepolymerized branched actin filaments resulted in debranching (Gandhi et al., 2010). At high concentrations, GMF can also compete with NPFs for Arp2/3 complex binding, preventing branch formation (Gandhi et al., 2010; Nakano et al., 2010). This is thought to occur through one interface on GMF blocking the NPF WCA domain C-helix binding site on the Arp2/3 complex (Ydenberg et al., 2013; Luan and Nolen, 2013). A separate site on GMF is responsible for its debranching activity, which occurs through destabilization of the Arp2/3–daughter filament junction (Luan and Nolen, 2013; Ydenberg et al., 2013). Supporting its role in actin turnover, depletion of GMF has been associated with accumulation of actin patches in yeast and peripheral F-actin in *Drosophila melanogaster* S2 cells and border cells (Nakano et al., 2010; Poukkula et al., 2014). Recent work in S2 cells shows that GMF localizes to the cell periphery, and its localization appears to increase upon retraction. Furthermore, border cells

The Rockefeller University Press $30.00
J. Cell Biol. Vol. 209 No. 6   803–812
www.jcb.org/cgi/doi/10.1083/jcb.201501094

JCB   803

depleted of GMF have reduced protrusion dynamics early after detachment from the epithelium (Poukkula et al., 2014).

The two vertebrate GMF isoforms (GMFγ and GMFβ) are present in a variety of tissues. GMFγ is highly expressed in immune cells and vascular endothelium (Ikeda et al., 2006; Zuo et al., 2013), whereas GMFβ has high expression in the brain and is ubiquitously expressed in other tissues, as revealed by RNaseq (Zuo et al., 2013; http://www.ebi.ac.uk/gxa/genes/ENSG00000197045). GMFγ has previously been implicated in leading edge dynamics, cell migration, and chemotaxis in multiple cell types (Ikeda et al., 2006; Aerbajinai et al., 2011; Lippert and Wilkins, 2012; Poukkula et al., 2014). Little work has been done on GMFβ, despite its homology to GMFγ. Here, we provide a systematic analysis of how GMFβ affects branched actin, lamellipodial behavior, and directional migration.

Results and discussion

GMFβ displays Arp2/3-dependent localization to the leading edge

GMFβ was the only GMF isoform expressed in our IA32 mouse embryonic fibroblasts (Fig. S1 A), but both isoforms share considerable similarity (Fig. S1 B). Because yeast GMF1 and GMFγ are reported to bind to the Arp2/3 complex, we reasoned that GMFβ should colocalize with branched actin at the leading edge. Indeed, GMFβ localized to lamellipodia when visualized by immunostaining for the endogenous protein (Fig. 1 A, top) or by expression of a GMFβ-GFP fusion (Fig. 1 A, bottom). This localization was lost in IA32 cells depleted of two subunits of the Arp2/3 complex, which lack lamellipodia (Fig. S1 C; Wu et al., 2012). To ensure that this localization was not an artifact of cell edge ruffling or increased volume at the cell edge, we used ratiometric imaging of cells expressing tRFP (a nonspecific volume marker) and either GFP alone, GMFβ-GFP, or a GFP-tagged subunit of Arp2/3 (p34-GFP). With this approach, GFP alone shows no specific edge localization (Fig. 1 B, left two panels; and Video 1), whereas both GMFβ-GFP (Fig. 1 B, center; and Video 1) and p34-GFP (Fig. 1 B, right; and Video 1) show an enhanced lamellipodial signal.

We suspected that GMFβ may localize to lamellipodia only at specific times during their protrusion cycle, as GMFβ did not localize as uniformly as other leading edge markers (Fig. 1 B). To synchronize lamellipodia, we used the small molecule inhibitor of Arp2/3, CK-666 (Nolen et al., 2009; Hetrick et al., 2013). Cells treated with CK-666 completely lost lamellipodia, which regrew in a synchronized manner upon drug washout (Fig. S2 A). Cells remained primarily in the protrusion phase for 10 min after washout, after which retraction and ruffling were observed (unpublished data). Although cortactin returns to the lamellipodia within 1 min of CK-666 washout, GMFβ localization is delayed, appearing by 5 min after washout (Fig. 1 C). GMFβ's delay in localization suggests that it does not affect the early protrusion phase, and that its localization may be dependent on the age of the branched actin network. This protrusion synchronization protocol was used in combination with contour-erosion–based intensity measurements along the lamellipodia (Fig. S1 D) to generate maps of the localization of either GMFβ-GFP or GFP alone after 10 min of CK-666 washout (Cai et al., 2007). While the maximum fluorescence intensity of GFP was measured toward the inside of cells (Fig. S1 E), the maximum GMFβ-GFP fluorescence intensity occurred at the edge
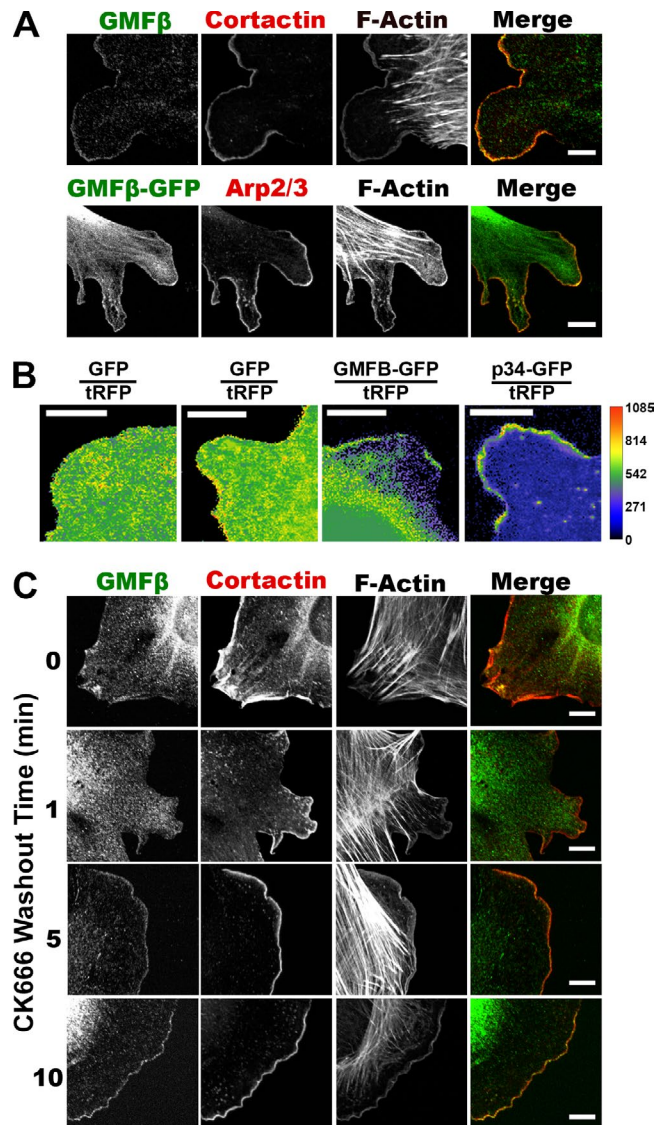

Figure 1. **GMFβ localizes to the leading edge of fibroblasts.** (A) GMFβ localization by immunofluorescence (IF; top) and in cells expressing GMFβ-GFP (bottom). Arp2/3 or cortactin IF marks leading edge. (B) Ratio of either soluble GFP, GMFβ-GFP, or p34-GFP to soluble RFP. The legend to the right represents pixel intensity. (C) IF for GMFβ and cortactin of cells treated with CK-666 (150 µM) to ablate lamellipodia, followed by washout for given times to allow lamellipodia regrowth. Bars, 10 µm

of cells in a similar pattern to Arp2/3 and actin (Fig. S1 F). These data indicate that GMFβ edge localization is specific and dependent on the presence of Arp2/3-branched actin filaments.

GMFβ is critical for lamellipodial retraction

We next assessed GMFβ's role in lamellipodial dynamics. Using lentiviral expression of an shRNA for GMFβ, we created a GMFβ-depleted cell line (KD), as well as a GMFβ-depleted cell line rescued with an shRNA-resistant GMFβ-GFP construct (KDR; Fig. 2 A). GMFβ was barely detectable (<1%) by Western blotting after shRNA expression (Fig. S1 G). An overexpression cell line (OE) was created by lentiviral infection of cells with a GMFβ-GFP construct followed by sorting for highly expressing cells (Fig. 2 A). The GMFβ-depleted cell line displayed a larger spread size with broad lamellipodia in comparison to control cells (CNTL), which
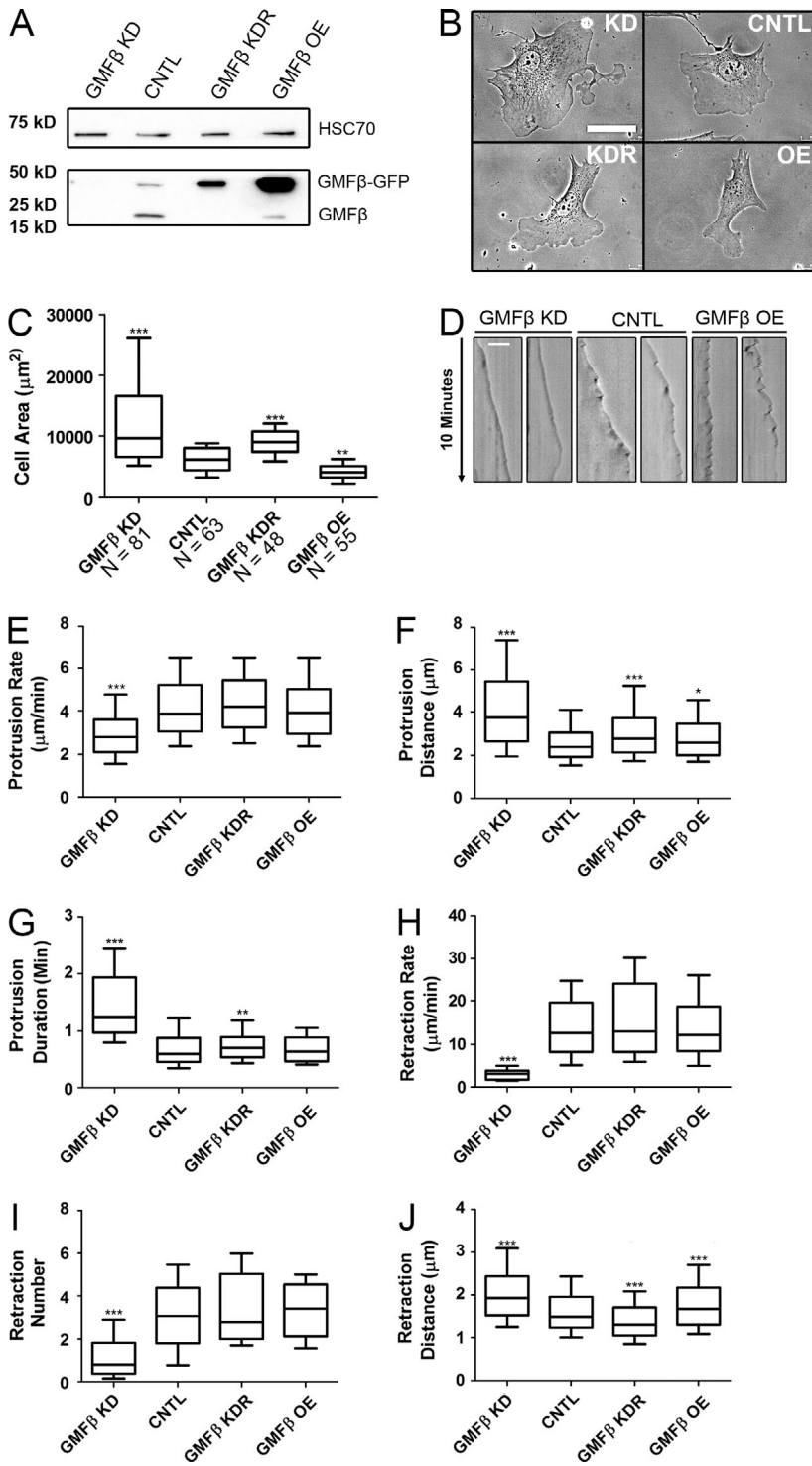
Figure 2. **Changes in GMFβ expression level alter cell shape and lamellipodial dynamics.** (A) Western blot showing GMFβ expression of created cell lines. (B) GMFβ-depleted (KD) and -overexpressing (OE) cells show phenotypic changes versus control (CNTL) and knockdown-rescue (KDR) cell lines. Bar, 50 μm. (C) Cell area quantified from micrographs. (D) Example kymographs for GMFβ KD, CNTL, and GMFβ OE. Bar, 10 μm. (E) Protrusion rate in micrometers per minute measured from kymography. (F) Protrusion distance in micrometers. (G) Protrusion duration in minutes. (H) Retraction rate in micrometers per minute. (I) Mean number of retractions per protrusion. (J) Retraction length in micrometers. For all graphs, error bars represent 10th–90th percentile. Kruskal-Wallis multiple comparison testing was performed, and significance was measured with a Dunn's post-test. ***, $P < 0.001$; **, $P < 0.01$; *, $P < 0.05$. $n \geq 20$.

could be rescued by expressing shRNA-resistant GMFβ (KDR; Fig. 2, B and C). Conversely, GMFβ-overexpressing cells had a lower spread area and smaller lamellipodia compared with control cells (Fig. 2, B and C). These lamellipodia also behaved differently: GMFβ-depleted cells had slower, less dynamic protrusions with little ruffling, whereas GMFβ-overexpressing cells had dynamic protrusions with frequent ruffling. We analyzed cells by kymography, which confirmed our visual impressions (Fig. 2 D). GMFβ-depleted cells had a decreased protrusion rate and an increased protrusion distance and duration (Fig. 2, E–G). More dramatically,

depletion of GMFβ produced a severe reduction in retraction rate and frequency that could be rescued by reexpression of GMFβ (Fig. 2, H and I). The observed increase in retraction and ruffling behavior in GMFβ-overexpressing cells was not due to an actual increase in retraction frequency (Fig. 2 I) but instead due to an increase in the distance of each retraction event (Fig. 2 J). To summarize, GMFβ-depleted cells retract slowly and less frequently, but for a longer total distance, whereas GMFβ-overexpressing cells retract at the same speed and as frequently as control cells, but for an increased distance per retraction (Fig. 2, H–J).

Arp2/3 localization and stability is influenced by GMFβ

We next tested for changes to the Arp2/3 complex content or dynamics by altering GMFβ expression. If GMFβ is "pruning" Arp2/3-based branches, it is plausible that width or density (represented by Arp2/3 intensity) of lamellipodial branched actin could be altered by GMFβ depletion or overexpression. We used edge intensity mapping (Fig. S1 D) to measure Arp2/3 complex intensity in protruding (synchronized) lamellipodia and in normally cycling (unsynchronized) lamellipodia. In synchronized populations there was no difference between GMFβ-depleted cells and control cells in the front-to-back width or intensity of Arp2/3 complex (Fig. 3 A, left). However, overexpression of GMFβ greatly reduced the Arp2/3 complex intensity in synchronized cells (Fig. 3 A, right).

When the same analysis was performed on unsynchronized GMFβ-depleted cells, an increase in the intensity of Arp2/3 complex at the cell edge was apparent, but the width of the branched actin network remained unchanged (Fig. 3 B, left). In unsynchronized GMFβ-overexpressing cells, however, Arp2/3 intensity remained reduced as in synchronized populations (Fig. 3 B, right). Because synchronization of lamellipodia allows analysis of cells actively engaged in protrusion, our data suggest that GMFβ-depleted cells generate branched actin similarly to control cells during this phase. In unsynchronized populations of lamellipodia, we are able to observe cells in mixed states of protrusion and retraction. Because GMFβ-depleted cells have an increased accumulation of Arp2/3 complex in an unsynchronized state, this accumulation may be due to a defect in their retraction phase.

Because we did not observe differences in the width of the branched actin network when GMFβ was depleted (despite visible differences in lamellipodia appearance and behavior), we hypothesized that GMFβ may instead control the distribution of Arp2/3 laterally. We immunostained synchronized cells to visualize the Arp2/3 complex (Fig. 3 C) and used a custom MATLAB script to generate heat maps of Arp2/3 along the cell edge (Fig. 3 C, insets) to determine the percentage of the cell perimeter positive for Arp2/3 signal above the mean Arp2/3 intensity of the entire cell. Using this analysis, we found that GMFβ-depleted cells had an increase in Arp2/3-positive cell perimeter compared with control cells, whereas GMFβ-overexpressing cells had a reduced Arp2/3-positive cell perimeter (Fig. 3 D).

GMFβ is thought to have two branch antagonizing activities: directly destabilizing the existing branch junction and preventing Arp2/3 activation by NPFs (Ydenberg et al., 2013; Luan and Nolen, 2013). The observed changes in Arp2/3 distribution could be due to either or both of these activities. If debranching is a main function of GMFβ, then depleting GMFβ should lead to observable changes in the branched actin disassembly rate. To measure this, we used CK-666 wash-in to stop creation of new branches while leaving existing branches unaffected (Hetrick et al., 2013; Fig. S1 H). Therefore, any decrease in Arp2/3 intensity at the leading edge represents the rate of branch disassembly. Using this technique in cells expressing a GFP-tagged subunit of Arp2/3 (Wu et al., 2012), we observed an increase in the stability of the Arp2/3 complex upon GMFβ depletion (Fig. 3 E and Video 2). This could be observed by measuring both the amount of cell edge positive for Arp2/3 (Fig. 3 F) and the intensity of Arp2/3 signal at the edge (Fig. 3 G). Although we cannot rule out NPF competition using this assay, it is notable that GMFβ-overexpressing cells do not display a comparable phenotype to CK-666–treated cells. If GMFβ is blocking activation of Arp2/3 by NPFs, GMFβ overexpression should mimic inhibiting Arp2/3 by CK-666 treatment. While cells treated with CK-666 lose lamellipodia entirely and become dominated by bundled actin structures (Fig. S2 A), GMFβ-overexpressing cells retain small dynamic lamellipodia with lower amounts of Arp2/3 complex (Fig. S2 B). Furthermore, if GMFβ acts to suppress Arp2/3 activation, we should see an increase in the intensity of Arp2/3 complex signal during the protrusion phase in synchronized GMFβ-depleted cells (Fig. 3 A, left). Instead, we only observed this increase in intensity when GMFβ-depleted cells are unsynchronized (Fig. 3 B, left). Together, these observations support debranching as the dominant role of GMFβ in our cells, and agree with recent in vitro studies showing that GMF had only weak inhibition of nucleation in the presence of the WCA domain of N-WASP, and no inhibition with the WCA domain of WAVE (Boczkowska et al., 2013).

Mutant GMFβ cannot rescue GMFβ depletion phenotypes

Ydenberg et al. (2013) created a series of mutations to assess which sites of budding yeast GMF1 were involved in debranching and NPF competition. Two distinct sites were identified: site 1 appears to be required for NPF competition, whereas both sites 1 and 2 are for necessary for debranching. Thus a mutation affecting only debranching could be created. The mutation that caused the largest debranching defect in budding yeast GMF1 was also created in mouse GMFγ, where R19, K20, and R22 were changed to alanines and showed defective debranching activity (Ydenberg et al., 2013). We generated analogous mutations in GMFβ (R19A, K20A, and R22A) to test if this mutant could rescue the defects observed in GMFβ-depleted fibroblasts (Fig. 4 A). We found that this mutant GMFβ localized to the leading edge, although less robustly than wild-type (WT) GMFβ-GFP (Fig. 4, B and C). We created cell lines with mutant GMFβ that were comparable to our existing WT GMFβ cell lines. In addition to overexpressing mutant GMFβ in cells, a second cell line was made in which endogenous GMFβ was depleted by shRNA expression and cells were "rescued" with an shRNA-resistant mutant GMFβ (Fig. S2 C). We first compared the overexpression of the mutant GMFβ to the overexpression of WT GMFβ. In contrast to the overexpression of WT GMFβ, overexpression of mutant GMFβ increased cell size, reduced lamellipodial retraction rate, and increased Arp2/3-positive cell edge (Fig. 4, D, F, and H). In the depletion-rescue experiment, expression of the mutant GMFβ construct did not rescue cell area, retraction rate, or the percentage of Arp2/3-positive cell edge (Fig. 4, E, G, and I). Kymography of protrusion characteristics showed similar, but less pronounced trends in the mutant's inability to rescue depletion of endogenous GMFβ or mimic overexpression of WT GMFβ (Fig. S2, D–I). This suggests that the debranching site of GMFβ is critical for its physiological role at the cell edge, and that defects in GMFβ-depleted cells result from the loss of debranching activity.

Branched actin pruning by GMFβ is important for whole cell motility and is necessary for haptotaxis, but not chemotaxis

We sought to determine whether GMFβ-related changes to lamellipodial dynamics affected whole cell migration. We found that depletion of GMFβ reduces cell velocity in sin-
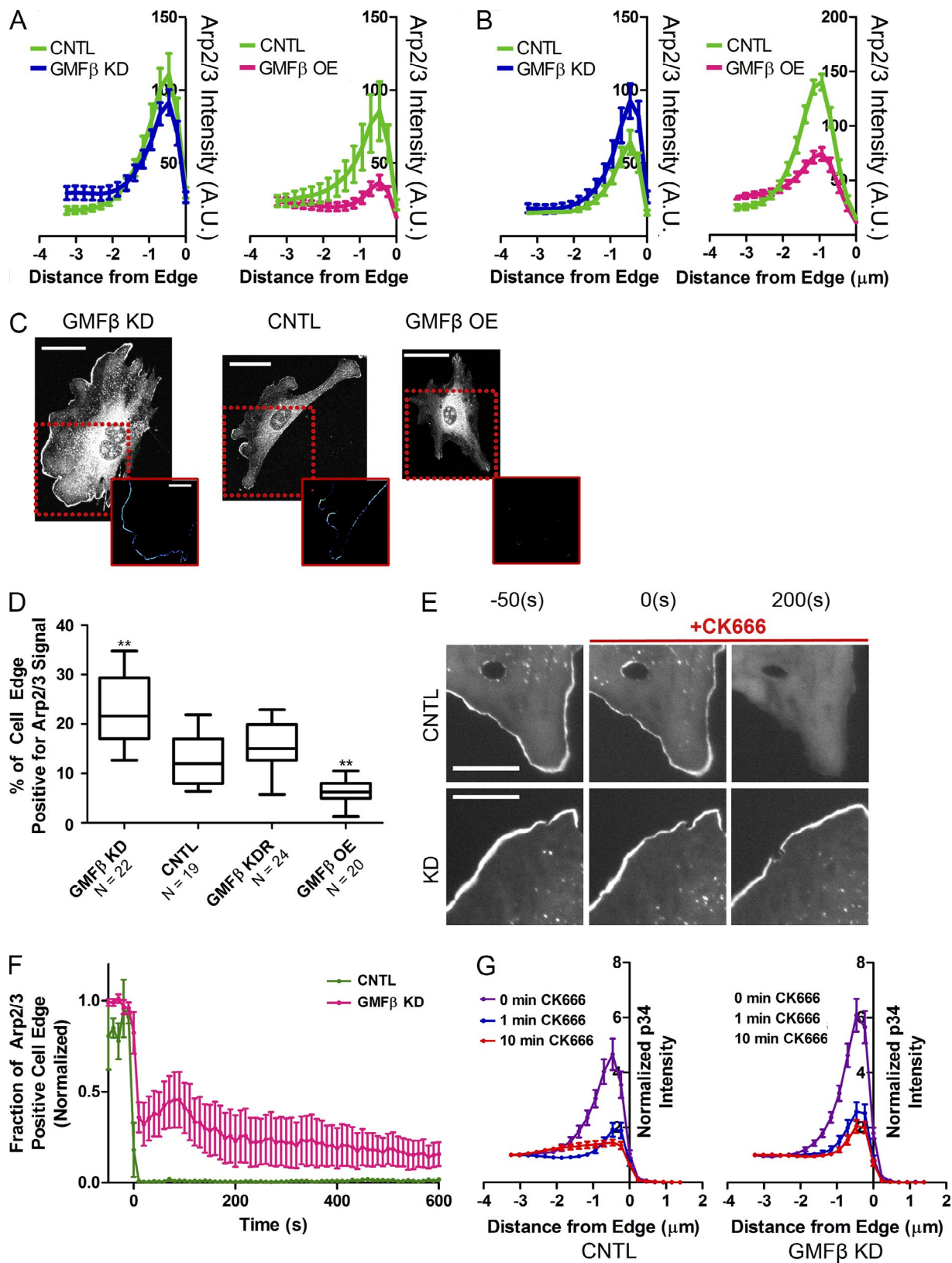
Figure 3. **GMFβ alters distribution and stability of Arp2/3 branched actin in the lamellipodium.** (A) Mapping of p34 (Arp2/3) intensity in synchronized lamellipodia of GMFβ KD (left) or GMFβ OE (right) versus CNTL. The cell edge is at 0. Error bars indicate SEM. (B) Mapping of p34 (Arp2/3) intensity in unsynchronized lamellipodia of GMFβ KD (left) or GMFβ OE (right) versus CNTL. The cell edge is at 0. Error bars indicate SEM. (C) Arp2/3 IF in GMFβ KD, CNTL, and GMFβ OE cells with synchronized lamellipodia. Insets represent a computer-generated map of high Arp2/3 edge signal for each image. Bars: (top) 50 μm; (bottom) 25 μm. (D) The percentage of cell edge positive for high Arp2/3 signal, generated from p34 IF. Error bars represent the 10th–90th percentile. A Kruskal-Wallis multiple comparison testing was performed, and significance was measured with a Dunn's post-test (***, $P < 0.001$; **, $P < 0.01$; *, $P < 0.05$). (E) Stills from a live-cell wash-in of CK666 on p34 knockdown cells rescued with p34-GFP (p34KDR). Control p34KDR cells (top)

gle cell tracking assays of randomly migrating cells, whereas overexpression of GMFβ increases it (Fig. 5 A). These effects were not observed in Arp2/3 complex–depleted cells, suggesting that GMFβ's effects on motility are Arp2/3 dependent (Fig. S3 A). Re-introduction of WT GMFβ into cells depleted of endogenous GMFβ rescued the observed defect in cell velocity (Fig. 5 A). Expression of mutant GMFβ, however, could neither rescue endogenous GMFβ depletion nor replicate the overexpression phenotype of WT GMFβ (Fig. S3, B and C).

To address the role of GMFβ in directional migration, we used microfluidic chambers to generate gradients where cells can be directly observed during migration toward environmental cues (Wu et al., 2012; Asokan et al., 2014). Control cells plated within the same chambers served as internal controls for all experiments, and forward migration index (FMI) was used as a measure of directional motility (Asokan et al., 2014). An FMI with 95% confidence intervals (indicated by error bars) encompassing 0 represents the inability to directionally migrate. We tested the ability of GMFβ-overexpressing and GMFβ-depleted cells to migrate toward soluble cues in the form of a gradient of PDGF (chemotaxis). Consistent with previous findings that Arp2/3-based actin assembly is dispensable for PDGF chemotaxis in fibroblasts (Wu et al., 2012), both GMFβ-overexpressing (Fig. 5 B) and GMFβ-depleted (Fig. 5 C) cells could migrate up a concentration gradient of PDGF as well as control cells. Next, we assayed GMFβ's effect on cells migrating on a gradient of surface-bound ECM (haptotaxis). GMFβ-overexpressing cells were unable to haptotax up a gradient of fibronectin in comparison to control cells (Fig. 5 D). Because GMFβ-overexpressing cells have less Arp2/3 at the leading edge (Fig. 3 A, right), this result agrees with previous data from our laboratory showing that cells depleted of the Arp2/3 complex could not haptotax (Wu et al., 2012). However, it is important to note that GMFβ-overexpressing cells still have lamellipodia containing some Arp2/3, showing that less severe interruption of branched actin can abrogate haptotaxis (Fig. S2 B). Cells depleted of GMFβ were also unable to haptotax (Fig. 5 E), despite having an increase in both peak Arp2/3 edge intensity and the percentage of Arp2/3-positive cell edge (Fig. 3, B and D). Again, reintroduction of GMFβ-GFP into GMFβ-depleted cells was able to rescue the defect in haptotaxis (Fig. 5 F). These data suggest that the presence of lamellipodia is not sufficient for haptotaxis, and proper regulation of branched actin in the lamellipodia is critical for sensing and/or responding to an ECM gradient.

This study supports debranching by GMFβ as a prominent mechanism in the regulation of branched actin, allowing for appropriate lamellipodial retraction and limiting lateral lamellipodial growth. GMFβ does not appear to have significant effects on the protrusion phase of lamellipodial growth, where the effects of NPF competition should be most apparent. GMFβ likely acts in concert with other debranching and actin-severing proteins (such as cofilin and coronins), as we observed a partial loss of Arp2/3 complex signal after CK-666 treatment in GMFβ-depleted cells (Fig. 3, F and G). This implies that there may be a specific fraction of actin branches

for which GMFβ is crucial for pruning, but other debranching mechanisms may operate in parallel.

Our observations highlight the importance of the proper regulation of lamellipodia in controlling cell motility. Systems for reinforcing desired lamellipodia and eliminating unproductive lamellipodia are likely crucial for efficient management of actin within the cell and efficient cell migration. Moreover, our results reinforce the critical role that lamellipodia play in sensing and responding to ECM cues. One of the key unanswered questions arising from this work is how GMFβ might be regulated. Mechanisms that activate or inhibit GMFβ's activity would provide a potent way to regulate lamellipodial behavior and, ultimately, whole cell motility.

Materials and methods

Reagents and materials
Commercial antibodies were purchased from EMD Millipore (mouse anti-cortactin, rabbit anti-p34-Arc), Sigma-Aldrich (rabbit anti-GMFβ [SAB2701114, Western blot; and HPA002954, immunofluorescence]), Takara Bio, Inc. (mouse anti-GFP), Santa Cruz Biotechnology, Inc. (mouse anti-HSC70), and Jackson ImmunoResearch Laboratories, Inc. (HRP-conjugated goat anti–mouse and goat anti–rabbit, Cy5, Cy2, and Rhodamine Red-X goat anti–rabbit, and Cy5 and Rhodamine Red-X goat anti–mouse secondary antibodies). Phalloidin was purchased from Life Technologies (Alexa Fluor 647, 568). Fibronectin for coating glass was purchased from BD. The Arp2/3 inhibitor CK-666 was purchased from EMD Millipore. Transfections were performed with X-tremeGENE (Roche).

Plasmids
GMFβ shRNA plasmid (TRCN0000108774) from the UNC Chapel Hill Lenti-shRNA Core Facility, which uses the GE Healthcare TRC1 shRNA library. The hairpin sequence for this plasmid (5′-CCGG-CGAGCTAACCAAGGTATTTGACTCGAGTCAAATACCTTG-GTTAGCTCGTTTTTG-3′) is contained on the pLKO.1 vector and controlled by a human U6 promoter. The pLKO.1 puromycin resistance cassette is under the control of the hPGK promoter. GMFβ-GFP fusion constructs were made by PCR amplification of GMFβ from an GMFβ cDNA construct from the Human ORFeome (Internal ID: 5592), followed by cut-and-paste cloning into our pLL 5.0 and pLL 7.0 LentiLox plasmids, where the gene was controlled by a 5′ UTR or CMV promoter, respectively. pLL5.0 was used for lower expressing cell lines (GMFβ KDR, mutant GMFβ), whereas pLL7.0 was used for overexpression. The mutant GMFβ construct was made by using overlap extension PCR to introduce the R19, K20, and R22 mutations into the gene. The nonspecific control hairpin target sequence is 5′-GATC-GACTTACGACGTTAT-3′, expressed in the pLL 5.0 plasmid. This sequence has no exact match in the human or mouse genome and has been previously characterized (Cai et al., 2007).

Cell culture
Previously generated mouse embryonic fibroblast lines (IA32) from an Ink4a/Arf$^{-/-}$ background were used as our base cell line (Wu et al., 2012). 2×KD cells, which Wu et al. (2012) generated by shRNA deple-

---

were compared with p34KDR cells depleted of GMFβ (bottom). CK-666 was added at 0 s. Bars, 25 µm. (F) Representative movies from E were analyzed to determine the percentage of the cell edge occupied by high Arp2/3 signal. CNTL n = 3, GMFβ KD n = 5. Error bars indicate SEM. (G) p34KDR WT and p34KDR cells depleted of GMFβ were treated with CK-666 for the listed times and fixed, then edge intensity of p34-GFP was measured for each time point. Error bars indicate SEM. 0 min n = 16 for both CNTL and KD, all other times n = 14 cells for both CNTL and KD.
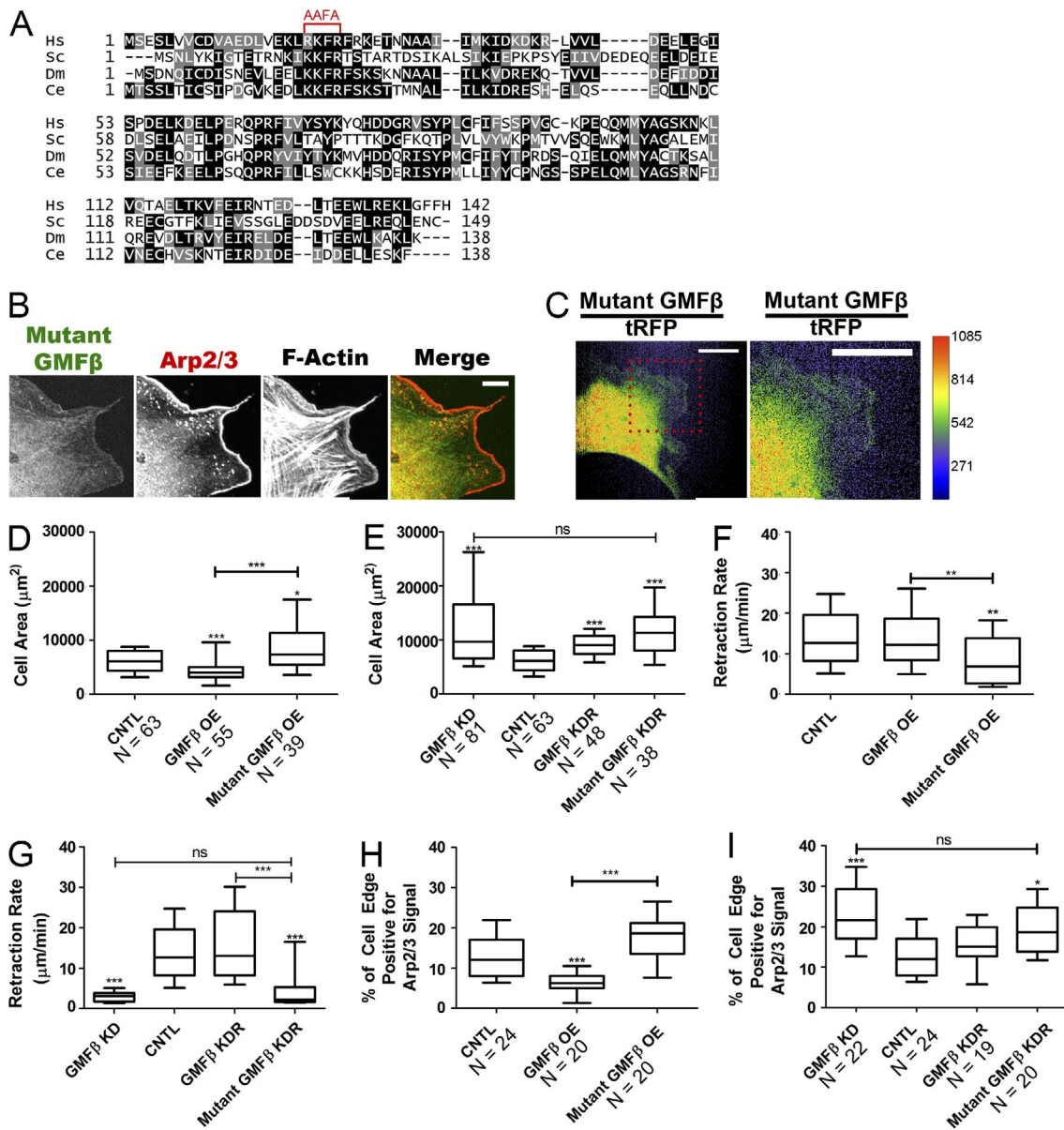
Figure 4. **Expression of a mutant GMFβ cannot rescue GMFβ depletion.** (A) Sequence alignment of human GMFβ (Hs) with *S. cerevisiae* (Sc), *Drosophila* (Dm), and *C. elegans* (Ce) GMF homologues. The mutated site is indicated by the red bracket. (B) Localization of mutant GMFβ-GFP in unsynchronized cells. IF of Arp2/3 and F-actin is shown. Bar, 10 µm. (C) Ratio of mutant GMFβ-GFP to soluble tRFP. The boxed region is enlarged on the right. Bars, 25 µm. (D) Cell area quantified from micrographs for mutant GMFβ OE. (E) Cell area quantified from micrographs for GMFβ KD cells rescued with mutant GMFβ (KDR). (F) Retraction rate in micrometers per minute for mutant GMFβ OE. (G) Retraction rate in micrometers per minute for mutant GMFβ KDR. (H) The percentage of cell edge positive for high Arp2/3 for mutant GMFβ OE. (I) The percentage of cell edge positive for high Arp2/3 for mutant GMFβ KDR. For all graphs, error bars represent 10th–90th percentile. Kruskal-Wallis multiple comparison testing was performed, and significance was measured with a Dunn's post-test. ***, P < 0.001; **, P < 0.01; *, P < 0.05.

tion of two subunits of Arp2/3 (p34Arc and Arp2) in IA32 cells, were also used (Figs. S1 C and S3 A). Cells were cultured in DMEM with 10% FBS, 100 U/ml penicillin, 100 µg/ml streptomycin, and 292 µg/ml ʟ-glutamine. This media was also used for any live cell imaging performed.

Lentiviral infection and FACs sorting

Cell lines were generated by lentiviral infection using the pLL5.0 or pLL7.0 vectors as described previously (Cai et al., 2007). In brief, the plasmid carrying the gene or shRNA of interest was cotransfected into Hek293-FT cells along with packaging vectors (Lois et al., 2002). Media was changed within 6–12 h of transfection, and virus was collected after 2 d. The virus is spun down to remove cell debris and applied to cells for 2 d, then removed. Lentivirally infected cells expressing fluorescent protein were collected by FACS with a cell sorter (S3; Bio-Rad Laboratories) into desired populations (top 10% for GMFβ-overexpressing cells, bottom 10% for cells used to make GMFβ KDR, all other lines sorted for all positive). Lentivirally infected cells expressing shRNA for GMFβ were selected by puromycin for 2 d at 2 µg/ml before use in assays. Control (CNTL) cells used in comparison with GMFβ shRNA knockdown lines were IA32 cells infected with a nonspecific shRNA hairpin and expressing a GFP marker. These cells were also used as control cells used in comparison with GMFβ-overexpressing lines in experiments where both GMFβ knockdown lines and overexpressing lines were being directly compared. Uninfected
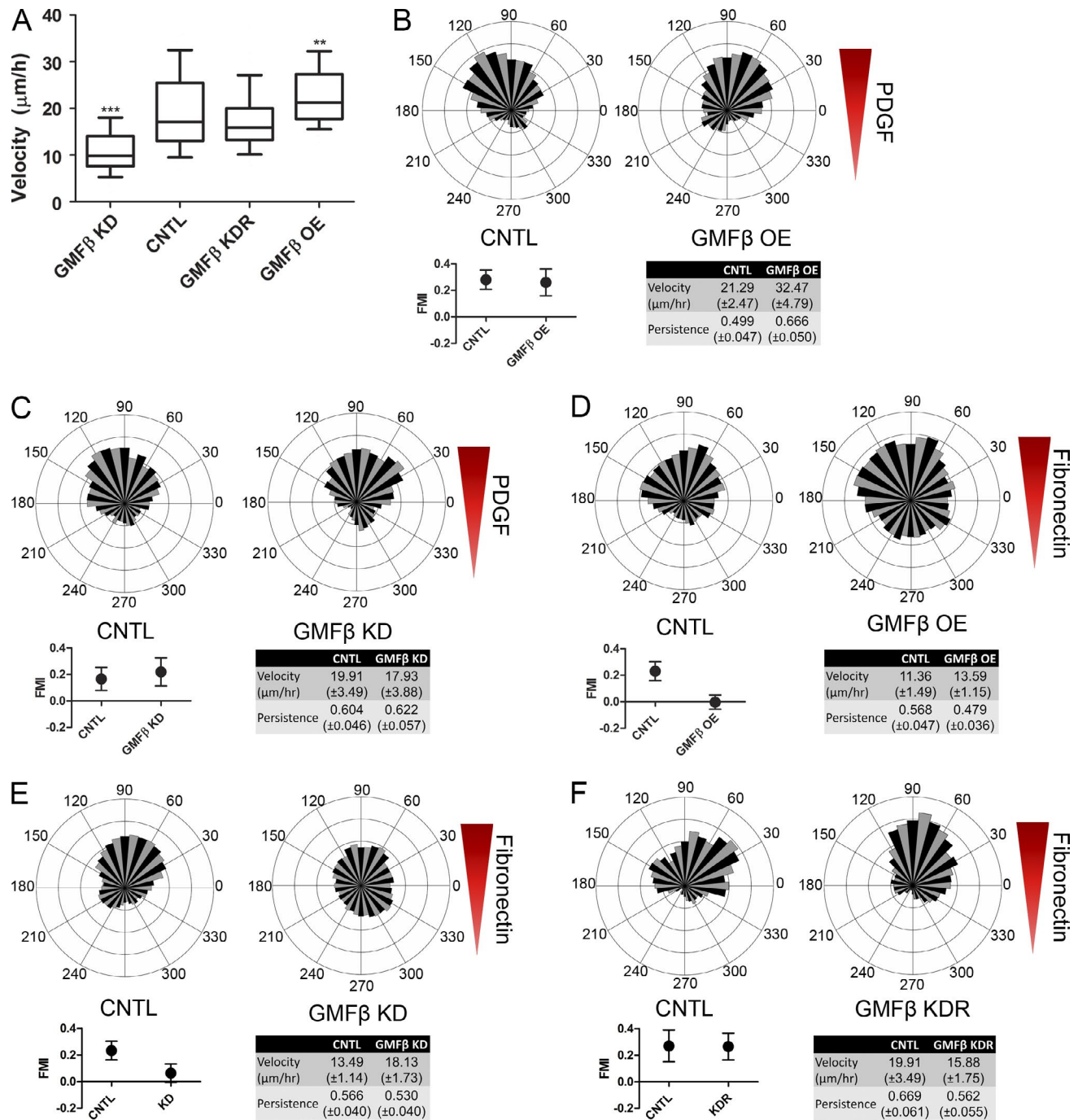
Figure 5. **Depletion or overexpression of GMFβ causes changes in whole cell velocity and defects in haptotaxis.** (A) Random migration velocity of single cells. Error bars represent the 10th–90th percentile. $n > 60$ for all conditions. Kruskal-Wallis multiple comparison testing was performed, and significance was measured with a Dunn's post-test. ***, $P < 0.001$; **, $P < 0.01$; *, $P < 0.05$. (B) Rose plots (top) for CNTL (left) and GMFβ OE (right) cells migrating in a PDGF gradient. FMI (bottom left), velocity, and persistence (bottom right table) are provided. FMI is plotted as the mean ± the 95% confidence interval. Values in the table are given as the mean with 95% confidence interval. CNTL $n = 89$, OE $n = 85$. (C) Rose plots (top) for CNTL (left) and GMFβ KD (right) cells migrating in a PDGF gradient. FMI, velocity, and persistence were provided as previously described (Asokan et al., 2014). CNTL $n = 118$, KD $n = 76$. (D) Rose plots (top) for CNTL (left) and GMFβ OE (right) cells migrating in a surface-bound fibronectin gradient. FMI, velocity, and persistence were provided as previously described. CNTL $n = 130$, OE $n = 208$. (E) Rose plots (top) for CNTL (left) and GMFβ KD (right) cells migrating in a surface-bound fibronectin gradient. FMI, velocity, and persistence were provided as previously described. CNTL $n = 144$, KD $n = 138$. (F) Rose plots (top) for CNTL (left) and GMFβ KDR (right) cells migrating in a surface-bound fibronectin gradient. FMI, velocity, and persistence were provided as previously described. CNTL $n = 41$, KDR $n = 59$.

wild-type IA32 cells were used as a control for GMFβ-overexpressing cells in experiments where GMFβ-depleted and GMFβ-overexpressing cells were not being directly compared (Fig. 3 A, right; Fig. 3 B, right; and Fig. 5, B and D).

Western blotting

Western blotting was performed in accordance with the standard technique (Rotty et al., 2015). Cells plated 70–80% confluent were washed with PBS and lysed by scraping with 4°C RIPA buffer containing pro-

tease inhibitors (1,10 phenanthroline and aprotinin, Sigma-Aldrich; Leupeptin, Roche). Blots for GMFβ were blocked in a mixture of 5% milk and 5% BSA to reduce background. Rabbit anti-GMFβ antibody (Sigma-Aldrich) was used at a 1:750 dilution and incubated overnight at 4°C. Blots were imaged using a ChemiDoc MP (Bio-Rad Laboratories) and analyzed using ImageLab 5.0. Representative blots are shown out of a set of at least three independent experiments.

Microscopy and image analysis

Immunofluorescence and lamellipodial synchronization. Cells were plated on coverslips coated with 10 µg/ml fibronectin and left to spread overnight before either being fixed with 4°C 4% PFA in Krebs-S buffer (for unsynchronized populations) or treated to synchronize lamellipodia. Lamellipodial synchronization was achieved by addition of 150 µM CK-666 for 2 h, followed by washout of the drug with regular DMEM for 10 min (unless otherwise specified) before fixation. Cells were then permeabilized in 0.1% Triton X-100 for 5 min. 5% BSA/NGS mixture was used to block for 1 h. Primary antibody was added either at 4°C overnight or for 2 h at room temperature. Secondary antibody was added for 1.5 h at room temperature. Coverslips were washed thoroughly with PBS and then mounted using Fluoromount-G (Electron Microscopy Sciences) or Fluorogel with Tris buffer (Electron Microscopy Sciences). In comparative experiments, control and test cells were plated in mixed populations on the same coverslip, and GFP expression or Cell Tracker dyes (Life Technologies) were used to identify populations. Coverslips were imaged on a confocal microscope (FV1000 or FV1200; Olympus) with a photomultiplier tube (Hamamatsu Photonics) controlled by Fluoview software (Olympus) with a 40× 1.3 NA objective lens (Olympus) at room temperature. Micrographs are displayed as maximum intensity projections of z stacks.

Ratio imaging. Cells stably expressing tagRFP-t were coinfected with either soluble GFP, GMFβ-GFP, mutant GMFβ-GFP, or p43-GFP. Cells were imaged on a confocal microscope (5-Live; Carl Zeiss) with a humidified environmental chamber (37°C, 5% CO_2) using a 63× 1.4 NA objective lens (Carl Zeiss) and a confocal microscope (LSM DuoScan; Carl Zeiss) controlled by LSM 5 software. Cells were imaged at 10-s intervals for 20 min. These movies were analyzed in ImageJ using the image calculator. The target of interest was set as the numerator, and the control protein (tagRFP-t) was set as the denominator. The resulting ratio image was then multiplied by a mask of the thresholded denominator to reduce background noise.

Edge mapping analysis. Edge mapping of leading edge proteins was performed using the ImageJ macro "Edgeratio" (Cai et al., 2007). In brief, maximum intensity projections were generated from confocal images of cells, and the projection for each channel imaged was combined into an RGB image. Regions which were positive for p34 (Arp2/3) or cortactin staining were considered lamellipodia and selected for analysis by a hand-drawn mask (Fig. S1 D). A threshold is generated to select the entire cell, and this selection is eroded or expanded to obtain average intensity values along the edge at various distances from the cell edge for each channel (Fig. S1 D). For GMFβ-GFP localization data, cells were unsynchronized and the signal was normalized to the peak fluorescence signal in the cell. Arp2/3 leading edge intensity measurements were performed on either p34 knockdown cells rescued with p34-GFP (p34-KDR; for GMFβ KD cells and their respective controls) or anti-p34 immunostaining (for GMFβ overexpressing [OE] cells and their respective controls). Arp2/3 (p34) intensity was presented raw and without normalization.

Kymography and random cell migration. Cells were plated overnight on glass-bottomed MatTek dishes coated with 10 µg/ml fibronectin. Cells used for kymography were imaged on a Biostation IM (Nikon) at 40× using 2-s intervals for 10 min. Kymographs were cre-

ated from movies in ImageJ using the Kymograph plugin (http://www.embl.de/eamnet/html/body_kymograph.html). Lines were drawn along protrusions and retractions, and the angles and lengths of these lines were recorded. A Perl script was used to analyze the data and output protrusion rates, etc. Random cell migration was also performed on the Biostation IM using the 20× objective. Cells were imaged for 12 h and then tracked using the Manual Tracking plugin for ImageJ (http://rsbweb.nih.gov/ij/plugins/track/track.html).

Cell size analysis. Phase micrographs of unsynchronized cells were manually outlined in ImageJ and the "measure" function was used to output the total cell area in square micrometers.

CK-666 wash-in. p34-KDR cells were plated overnight in 8-well chamber slides (Thermo Fisher Scientific) coated with 10 µg/ml fibronectin. Holes were punched through the lid of the chamber slide to allow tubing to be inserted, and this was connected to a syringe filled with CK-666 at 300 µM. An equal volume of CK-666–containing media was washed into the existing media in the well to achieve a final concentration of 150 µM. Cells were imaged with epifluorescence in a humidified environmental chamber (37°C, 5% CO_2) on a microscope (IX81; Olympus) using a 60×, 1.49 NA objective lens and a camera (Orca-ER; Hamamatsu Photonics) controlled by MetaMorph software (Molecular Devices). Images were captured at 5-s intervals as drug was applied, and imaging continued for at least 20 min after addition. The resulting live cell movies were analyzed for the percentage of Arp2/3 complex–positive edge (see Materials and methods). Because this experiment only allowed us to image a single cell at a time, we also performed a CK-666 wash-in on p34-KDR cells plated on fibronectin-coated coverslips. These cells were treated with CK-666–containing media for 1 or 10 min and then fixed immediately. Cells were stained with anti-GFP antibody, mounted, and imaged via confocal microscopy as described previously. p34-GFP intensity was measured from these images using the Edgeratio macro and normalized to the first data point (at −3.25 µm from the edge).

Percentage of Arp2/3 complex–positive edge analysis. Maximum-intensity projections of synchronized cells immunostained for the p34 subunit of the Arp2/3 complex were generated as described, and these images were analyzed using a MATLAB (MathWorks) program. K-means clustering was used to automatically segment the cell. A 10-pixel ring around the cell perimeter was defined, and the Arp2/3 signal at least 0.8 standard deviations above the mean was detected. The amount of cell edge marked by this high Arp2/3 signal was divided by the total perimeter of the cell, then multiplied by 100 to calculate the percentage of Arp2/3-positive cell edge.

Directional migration assays. Directional migration assays were performed as described previously (Wu et al., 2012, 2013). In brief, PDMS chambers containing microcapillaries were used to establish a gradient by flowing attractant in the source chamber, and a neutral media in the sink chamber. A constant flow of PDGF was used for the chemotactic gradient, whereas a fibronectin gradient was established for haptotaxis. Control and test cells were plated together in the central chamber containing the gradient, and GFP expression or cell dyes were used to distinguish populations. For chemotaxis experiments, cells were imaged for 24 h using a 20× Olympus objective lens on an inverted microscope (IX81; Olympus) with a humidified environmental chamber (37°C, 5% CO_2) and camera (Orca-ER; Hamamatsu Photonics) controlled by MetaMorph software. For haptotaxis experiments, cells were imaged for 16 h on an incubator microscope system (Vivaview, Olympus; humidified, 37°C, 5% CO_2) using a 20× 0.75 NA objective lens with magnification set to 0.5×, which was controlled by MetaMorph. Cells were tracked using the "Manual Tracking" plugin for ImageJ and these tracks were analyzed with the Chemotaxis Tool plugin from Ibidi to obtain forward migration index, persistence, and

velocity measurements. Rose plots were generated using the secplot script for MATLAB (http://www.mathworks.com/matlabcentral/fileexchange/14174-secplot).

Statistical analysis. All statistical analysis on generated data were performed using the software Prism (GraphPad Software). Error bars on boxplots represent the 10th–90th percentiles. Error bars on xy plots represent the standard error of the mean. Error bars on forward migration index plots represent the 95% confidence intervals. Box plot data were analyzed using the Kruskal-Wallis test to determine that individual samples did not come from identical populations. Statistical significance was determined by a Dunn's post-test after the Kruskal-Wallis test was performed.

Online supplemental material

Fig. S1 shows information relevant to GMFβ localization and expression in our cell lines, as well as details on the CK-666 wash-in experimental design. Fig. S2 shows the effects of CK-666 treatment of our cell lines, as well as information relevant to Fig. 4. Fig. S3 shows random cell migration velocity measurements supplemental to Fig. 5. Video 1 displays ratio imaging of a protein of interest (in GFP) to a nonspecific fill (RFP), related to Fig. 1 B. Video 2 is a live cell movie of CK-666 wash-in, relevant to Fig. 3 (E and F). kmeans1 m is an accessory file to arp23edge m, which allows kmeans clustering for detecting the outlines of cells. colormapb mat is a color map, which assigns colors to pixel intensities generated by the arp23edge m program. EdgeRatio is an ImageJ macro for analyzing the localization of proteins along the leading edge. KymoRate is a Perl script used for analyzing kymography data. PercentEdge is a MATLAB script used for analyzing the percentage of the cell perimeter positive for fluorescent signal. Online supplemental material is available at http://www.jcb.org/cgi/content/full/jcb.201501094/DC1.

References

Aerbajinai, W., L. Liu, K. Chin, J. Zhu, C.A. Parent, and G.P. Rodgers. 2011. Glia maturation factor-γ mediates neutrophil chemotaxis. *J. Leukoc. Biol.* 90:529–538. http://dx.doi.org/10.1189/jlb.0710424

Asokan, S.B., H.E. Johnson, A. Rahman, S.J. King, J.D. Rotty, I.P. Lebedeva, J.M. Haugh, and J.E. Bear. 2014. Mesenchymal chemotaxis requires selective inactivation of myosin II at the leading edge via a noncanonical PLCγ/PKCα pathway. *Dev. Cell.* 31:747–760. http://dx.doi.org/10.1016/j.devcel.2014.10.024

Boczkowska, M., G. Rebowski, and R. Dominguez. 2013. Glia maturation factor (GMF) interacts with Arp2/3 complex in a nucleotide state-dependent manner. *J. Biol. Chem.* 288:25683–25688. http://dx.doi.org/10.1074/jbc.C113.493338

Cai, L., T.W. Marshall, A.C. Uetrecht, D.A. Schafer, and J.E. Bear. 2007. Coronin 1B coordinates Arp2/3 complex and cofilin activities at the leading edge. *Cell.* 128:915–929. http://dx.doi.org/10.1016/j.cell.2007.01.031

Cai, L., A.M. Makhov, D.A. Schafer, and J.E. Bear. 2008. Coronin 1B antagonizes cortactin and remodels Arp2/3-containing actin branches in lamellipodia. *Cell.* 134:828–842. http://dx.doi.org/10.1016/j.cell.2008.06.054

Chan, C., C.C. Beltzner, and T.D. Pollard. 2009. Cofilin dissociates Arp2/3 complex and branches from actin filaments. *Curr. Biol.* 19:537–545. http://dx.doi.org/10.1016/j.cub.2009.02.060

Gandhi, M., B.A. Smith, M. Bovellan, V. Paavilainen, K. Daugherty-Clarke, J. Gelles, P. Lappalainen, and B.L. Goode. 2010. GMF is a cofilin homolog that binds Arp2/3 complex to stimulate filament debranching and inhibit actin nucleation. *Curr. Biol.* 20:861–867. http://dx.doi.org/10.1016/j.cub.2010.03.026

Hetrick, B., M.S. Han, L.A. Helgeson, and B.J. Nolen. 2013. Small molecules CK-666 and CK-869 inhibit actin-related protein 2/3 complex by blocking an activating conformational change. *Chem. Biol.* 20:701–712. http://dx.doi.org/10.1016/j.chembiol.2013.03.019

Ikeda, K., R.K. Kundu, S. Ikeda, M. Kobara, H. Matsubara, and T. Quertermous. 2006. Glia maturation factor-γ is preferentially expressed in microvascular endothelial and inflammatory cells and modulates actin cytoskeleton reorganization. *Circ. Res.* 99:424–433. http://dx.doi.org/10.1161/01.RES.0000237662.23539.0b

Lim, R., J.F. Miller, and A. Zaheer. 1989. Purification and characterization of glia maturation factor beta: a growth regulator for neurons and glia. *Proc. Natl. Acad. Sci. USA.* 86:3901–3905. http://dx.doi.org/10.1073/pnas.86.10.3901

Lippert, D.N., and J.A. Wilkins. 2012. Glia maturation factor gamma regulates the migration and adherence of human T lymphocytes. *BMC Immunol.* 13:21. http://dx.doi.org/10.1186/1471-2172-13-21

Lois, C., E.J. Hong, S. Pease, E.J. Brown, and D. Baltimore. 2002. Germline transmission and tissue-specific expression of transgenes delivered by lentiviral vectors. *Science.* 295:868–872. http://dx.doi.org/10.1126/science.1067081

Luan, Q., and B.J. Nolen. 2013. Structural basis for regulation of Arp2/3 complex by GMF. *Nat. Struct. Mol. Biol.* 20:1062–1068. http://dx.doi.org/10.1038/nsmb.2628

Nakano, K., H. Kuwayama, M. Kawasaki, O. Numata, and M. Takaine. 2010. GMF is an evolutionarily developed Adf/cofilin-super family protein involved in the Arp2/3 complex-mediated organization of the actin cytoskeleton. *Cytoskeleton (Hoboken).* 67:373–382.

Nolen, B.J., N. Tomasevic, A. Russell, D.W. Pierce, Z. Jia, C.D. McCormick, J. Hartman, R. Sakowicz, and T.D. Pollard. 2009. Characterization of two classes of small molecule inhibitors of Arp2/3 complex. *Nature.* 460:1031–1034. http://dx.doi.org/10.1038/nature08231

Pollard, T.D. 2007. Regulation of actin filament assembly by Arp2/3 complex and formins. *Annu. Rev. Biophys. Biomol. Struct.* 36:451–477. http://dx.doi.org/10.1146/annurev.biophys.35.040405.101936

Poukkula, M., M. Hakala, N. Pentinmikko, M.O. Sweeney, S. Jansen, J. Mattila, V. Hietakangas, B.L. Goode, and P. Lappalainen. 2014. GMF promotes leading-edge dynamics and collective cell migration in vivo. *Curr. Biol.* 24:2533–2540. http://dx.doi.org/10.1016/j.cub.2014.08.066

Rotty, J.D., C. Wu, and J.E. Bear. 2013. New insights into the regulation and cellular functions of the ARP2/3 complex. *Nat. Rev. Mol. Cell Biol.* 14:7–12. http://dx.doi.org/10.1038/nrm3492

Rotty, J.D., C. Wu, E.M. Haynes, C. Suarez, J.D. Winkelman, H.E. Johnson, J.M. Haugh, D.R. Kovar, and J.E. Bear. 2015. Profilin-1 serves as a gatekeeper for actin assembly by Arp2/3-dependent and -independent pathways. *Dev. Cell.* 32:54–67. http://dx.doi.org/10.1016/j.devcel.2014.10.026

Rouiller, I., X.-P. Xu, K.J. Amann, C. Egile, S. Nickell, D. Nicastro, R. Li, T.D. Pollard, N. Volkmann, and D. Hanein. 2008. The structural basis of actin filament branching by the Arp2/3 complex. *J. Cell Biol.* 180:887–895. http://dx.doi.org/10.1083/jcb.200709092

Wu, C., S.B. Asokan, M.E. Berginski, E.M. Haynes, N.E. Sharpless, J.D. Griffith, S.M. Gomez, and J.E. Bear. 2012. Arp2/3 is critical for lamellipodia and response to extracellular matrix cues but is dispensable for chemotaxis. *Cell.* 148:973–987. http://dx.doi.org/10.1016/j.cell.2011.12.034

Wu, C., E.M. Haynes, S.B. Asokan, J.M. Simon, N.E. Sharpless, A.S. Baldwin, I.J. Davis, G.L. Johnson, and J.E. Bear. 2013. Loss of Arp2/3 induces an NF-κB–dependent, nonautonomous effect on chemotactic signaling. *J. Cell Biol.* 203:907–916. http://dx.doi.org/10.1083/jcb.201306032

Ydenberg, C.A., S.B. Padrick, M.O. Sweeney, M. Gandhi, O. Sokolova, and B.L. Goode. 2013. GMF severs actin-Arp2/3 complex branch junctions by a cofilin-like mechanism. *Curr. Biol.* 23:1037–1045. http://dx.doi.org/10.1016/j.cub.2013.04.058

Zuo, P., Z. Fu, T. Tao, F. Ye, L. Chen, X. Wang, W. Lu, and X. Xie. 2013. The expression of glia maturation factors and the effect of glia maturation factor-γ on angiogenic sprouting in zebrafish. *Exp. Cell Res.* 319:707–717. http://dx.doi.org/10.1016/j.yexcr.2013.01.004